Electronic Supplementary Information (ESI)

Silk-based systems for highly efficient photothermal conversion under one sun: Portability, flexibility, and durability

Qian Zhang[a,b†], Xingfang Xiao[b†], Gang Wang[a], Xing Ming[a], Xinghang Liu[a], Han Wang[b], Hongjun Yang[b], Weilin Xu[*,b], and Xianbao Wang[*,a]

a. Hubei Collaborative Innovation Center for Advanced Organic Chemical Materials, Key Laboratory for the Green Preparation and Application of Functional Materials, Ministry of Education, Hubei Key Laboratory of Polymer Materials, School of Materials Science and Engineering, Hubei University, Wuhan 430062, P. R. China

b. State Key Laboratory of New Textile Materials & Advanced Processing Technologies and Hubei Key Laboratory of Advanced Textile Materials & Application, Wuhan Textile University, Wuhan 430200, P. R. China

† These authors contributed equally to this work.

*Corresponding author Email: weilin_xu0@163.com,wangxb68@aliyun.com

ESI Methods of material characterization

ESI-1. Morphology characterization

The morphologies of the silk fabric, GO–silk-fabric, and RGO–silk-fabric were observed using a field-emission scanning electron microscope (FESEM; Sigma 500, Zeiss, Germany) operating at 3 kV and a transmission electron microscope (TEM; Tecnai G2F30, FEI, USA). The cross sections of the silk fibers were prepared in two steps: each silk fiber was embedded

in resin, and the embedded sample was sectioned by a microtome along the cross section of the fiber.

ESI-2. FT-IR, XPS. and Raman measurements

The silk fabric, GO–silk-fabric, and RGO–silk-fabric were characterized by Fourier transform infrared (FT-IR) spectroscopy (iS50, Nicolet, USA). X-ray photoelectron spectroscopy (XPS) was carried out on an XP spectrometer (ESCALAB 250Xi, Thermo Fisher Scientific, USA). The Raman spectra were obtained using a confocal Raman spectrometer (inVia, Renishaw, UK) at an excitation wavelength of 532 nm.

ESI-3. Thermogravimetric analysis

A thermal analyzer (LABSYS evo, Setaram Instrumentation, France) was used for thermogravimetric (TG) analysis of samples from 30 to 800 °C, at a heating rate of 10 °C min^{-1} under nitrogen gas atmosphere.

ESI-4. Absorption of sun light

The absorption performance was measured in the wavelength range of 300 to 2500 nm using an ultraviolet–visible spectrophotometer (Lambda 950, PerkinElmer, USA) equipped with an integration sphere. The integrating sphere was used to collect the scattered light for accurate measurements.

ESI-5. Air permeability

The air permeability of the pristine silk fabric and RGO–silk-fabric was measured with an air permeability tester (G321, Gellowen Science, UK) through a given area (38 cm^2) of the fabric at a given pressure (100 MPa).

ESI-6. Mechanical properties

The mechanical properties were measured using a materials testing machine (Model 5566, Instron, USA) at a strain rate of 20 mm min^{-1}. For each measurement, five samples were tested and the mean value was used.

ESI-7. Solar-powered steam generation

The thermal images were captured by an infrared camera (FLIR E4, FLIR, USA). The light was generated by a xenon lamp (CELHXF300, Education Au-light Co Beijing, China). In order to verify the light-to-heat conversion properties of the samples, we compared different samples, including pure water, the GO–silk-fabric, and the RGO–silk-fabric. Solar irradiation was simulated on the basis of a white-light source by using a solar-simulator xenon lamp with a light density of 1 kW m^{-2}. During 30 min of irradiation, the mass of water in the beaker was recorded by an electronic balance. (The beaker was wrapped in polyurethane foam (thickness: 26 mm) as a heat-insulating wall to reduce thermal loss.) The weight change of water in different samples was calculated accordingly. To confirm the reusability of the system, the steam generation process of the RGO–silk-fabric was measured by recording the mass change as a function of time, and the evaporation examination was repeated 15 times under the same conditions. For each cycle, the RGO–silk-fabric was illuminated under a white-light source by the solar-simulator xenon lamp with a light density of 1 kW m^{-2}. After 30 min, the wetted RGO–silk-fabric was dried and re-arranged for the next cycle.

ESI-8. Durability to washing

The durability of the RGO–silk-fabric to washing was carried out according to the Chinese standard GB/T 12490-2007. A standard color-fast washing machine (Model SW-LZA, Changzhou Dahua Electronic Instrument Co., Ltd., China) was used to launder the fabric. The RGO–silk-fabric (5 × 5 cm) was washed at 50 °C for 30 min in a rotating closed canister

containing 150 mL of aqueous detergent solution (4 g L^{-1}); the above is considered as one washing cycle. A computer color-matching system (Color i7; X-Rite, USA) was used to measure the *K*/*S* value of the RGO–silk-fabric after washing.

ESI-Video S1. Capillary effect of pristine silk fabric and RGO–silk-fabric.
ESI-Video S2. Water supply by RGO–silk-fabric.
ESI-Video S3. Vapor generation by RGO–silk-fabric under one sun irradiation.
ESI-Video S4. Flexibility of RGO–silk-fabric.

ESI-Fig. S1 to Figure S10

Fig. S1. Optical images of pristine silk fabric, RGO–silk-fabric without sonication, and RGO–silk-fabric after sonication.
Fig. S2. Cross-sectional TEM image of RGO-silk fibers.
Fig. S3. Raman spectra of pristine silk fabric, GO–silk-fabric, and RGO–silk-fabric, obtained with an excitation wavelength of 532 nm.
Fig. S4. Thermogravimetric curves of pristine silk fabric and RGO–silk-fabric.
Fig. S5. Weight measurement process for pristine silk fabric and RGO–silk-fabric; the inset shows an optical image of pristine silk fabric and RGO–silk-fabric.
Fig. S6. Capillary effect of pristine silk fabric and RGO–silk-fabric.
Fig. S7. Optical images of RGO–silk-fabric floating on the surface of water (a) without and (b) with the insulating polyethylene foam (PEF). (Left: top view; right: side view)
Fig. S8. Evaporation mass loss of RGO–silk-fabric with and without PEF under one sun solar irradiation for 30 min.
Fig. S9. Surface temperatures of pure water, pristine silk fabric, GO–silk-fabric, and RGO–silk-fabric before and after solar irradiation. The entire water-temperature distribution after irradiation was monitored by an infrared camera.
Fig. S10. Evaporation mass loss of water in dark and at 1 sun.
Fig. S11. Comparison of photothermal-conversion efficiencies of our samples and previously reported carbon materials under one sun irradiation.
Fig. S12. The weight change of RGO-silk-fabric after cycles of use
Fig. S13. (a) Evaporation mass loss of pure water and simulated seawater (3.5 wt% NaCl solution) with RGO-silk-fabric under one sun solar irradiation for 30 min; (b) the corresponding evaporation rate of pure water and simulated seawater (3.5 wt% NaCl solution); (c) the salt concentration comparison; (d) a progression of salt precipitation on the surface of RGO-silk-fabric under one sun solar.
Fig. S14. A refractometer used to test the concentration of the dissolved salt in water.

ESI- Table S1 to Table S2

Table S1. Peak areas in C 1s spectra of GO–silk-fabric and RGO–silk-fabric.
Table S2. Mechanical properties of pristine silk fabric and RGO–silk-fabric.

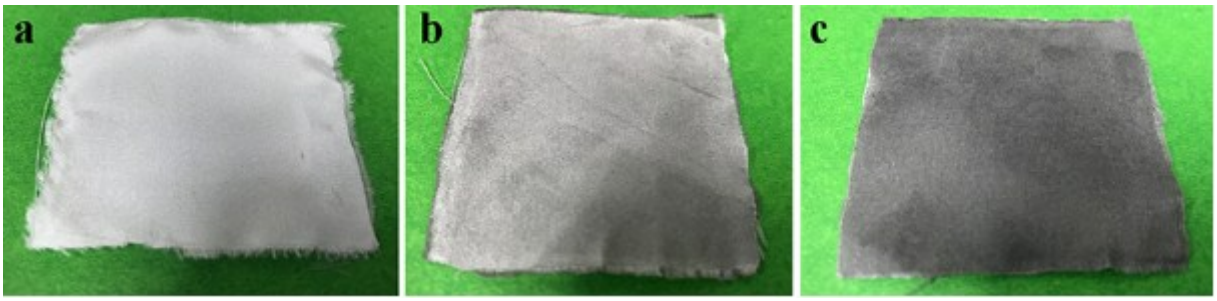

Fig. S1. Optical images of pristine silk fabric, RGO–silk-fabric without sonication, and RGO–silk-fabric after sonication.

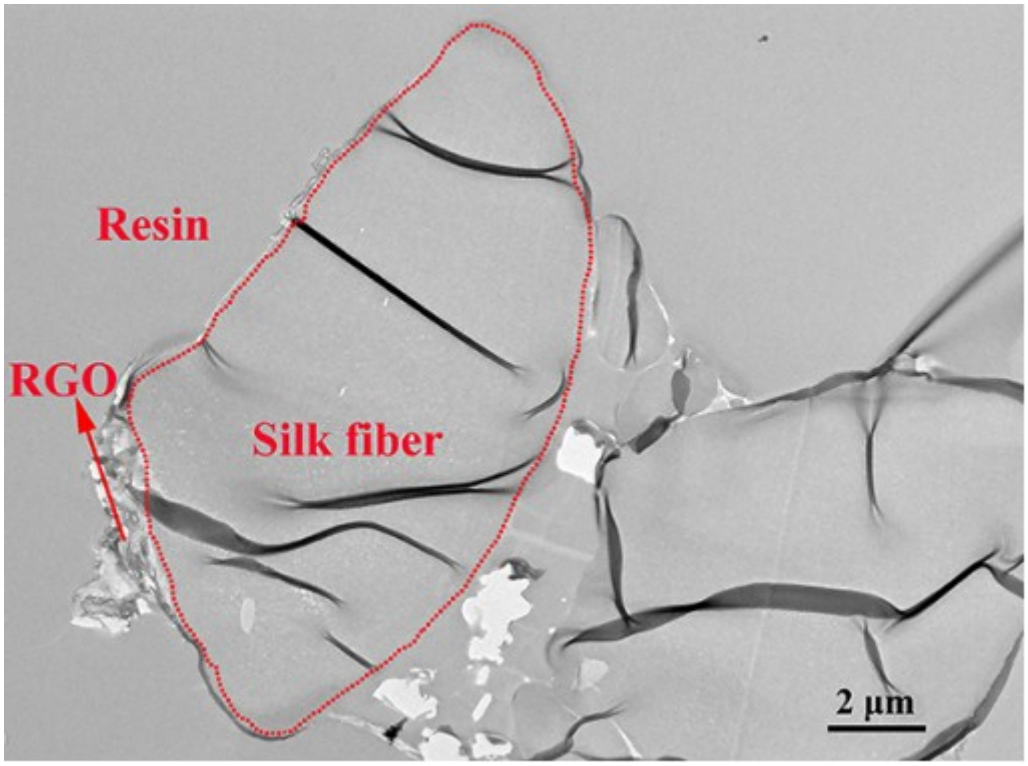

Fig. S2. Cross-sectional TEM image of RGO-silk fibers.

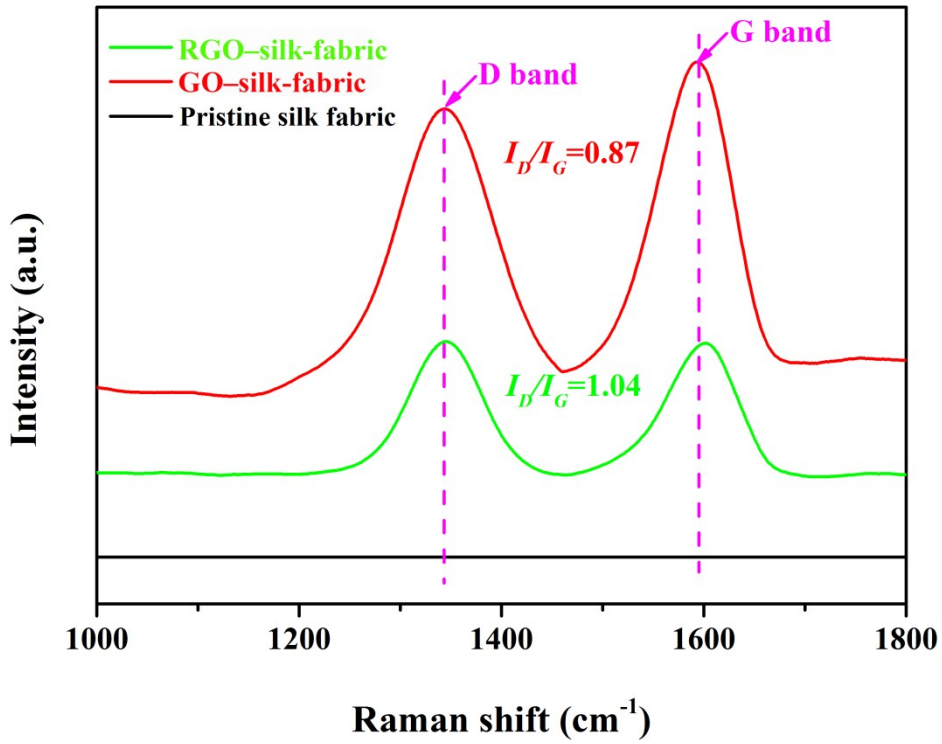

Fig. S3. Raman spectra of pristine silk fabric, GO–silk-fabric, and RGO–silk-fabric, obtained with an excitation wavelength of 532 nm.

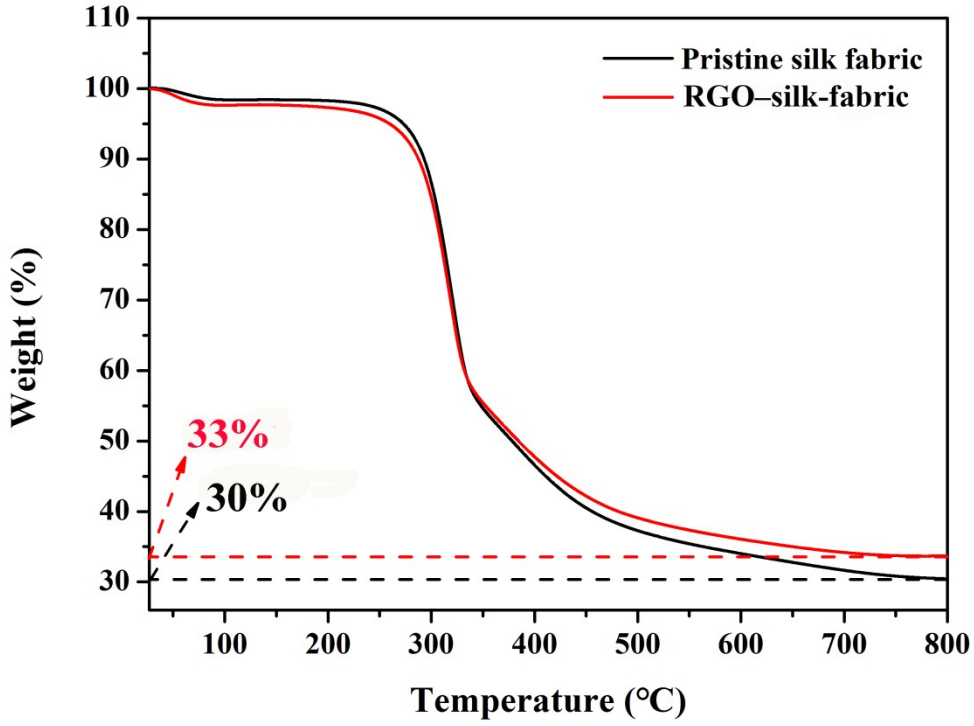

Fig. S4. Thermogravimetric curves of pristine silk fabric and RGO–silk-fabric.

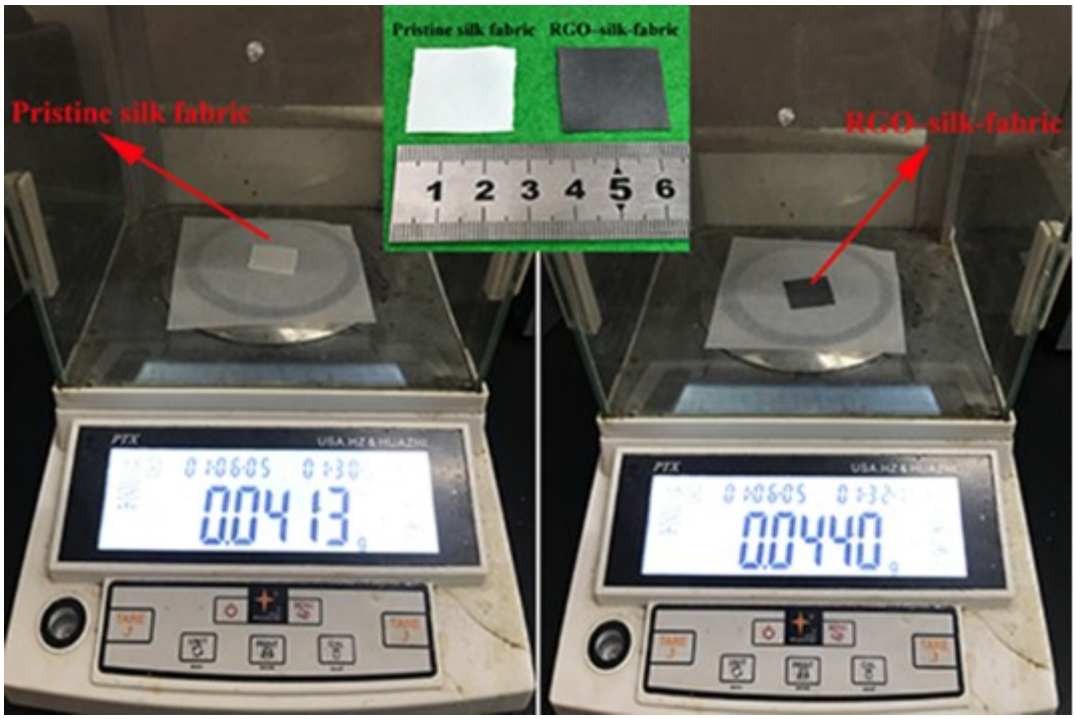

Fig. S5. Weight measurement process for pristine silk fabric and RGO–silk-fabric; the inset shows an optical image of pristine silk fabric and RGO–silk-fabric.

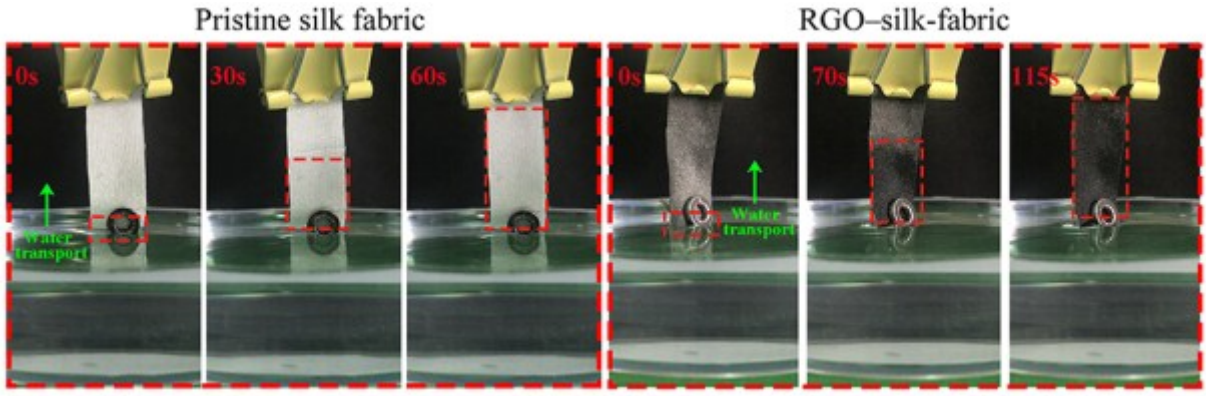

Fig. S6. Capillary effect of pristine silk fabric and RGO–silk-fabric.

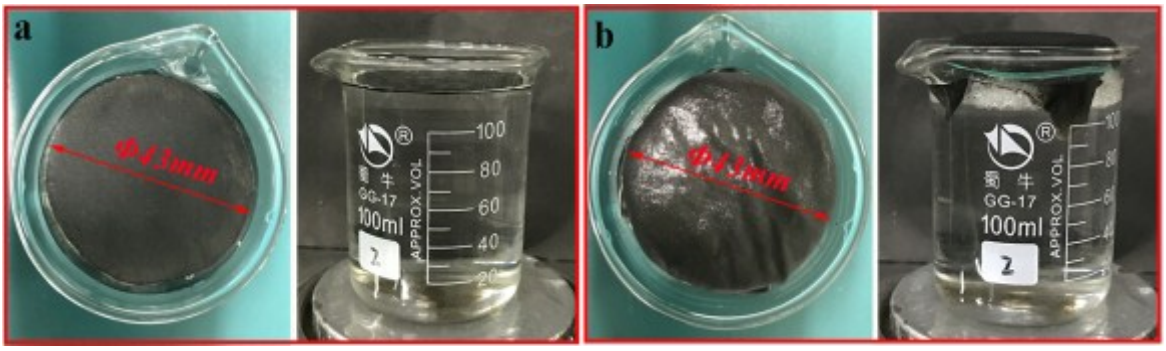

Fig. S7. Optical images of RGO–silk-fabric floating on the surface of water (a) without and (b) with the insulating polyethylene foam (PEF). (Left: top view; right: side view)

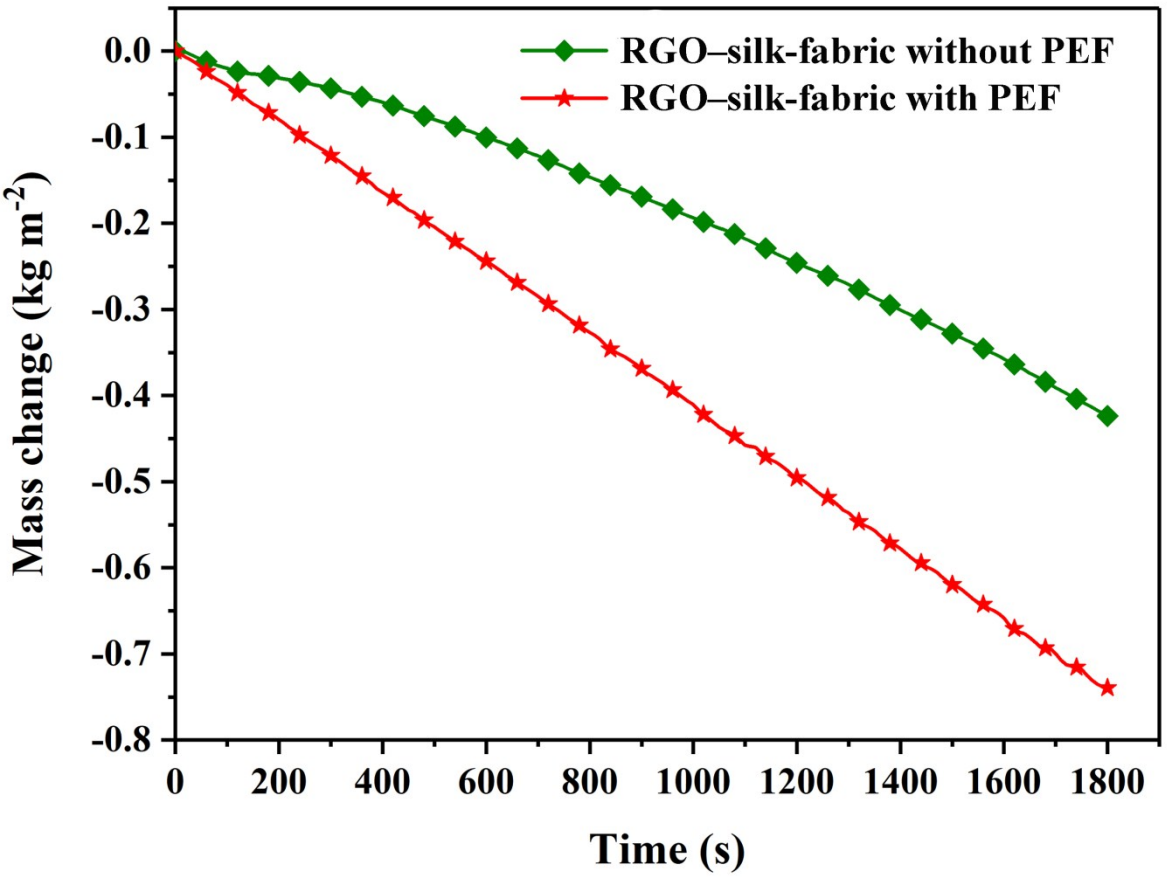

Fig. S8. Evaporation mass loss of RGO–silk-fabric with and without PEF under one sun solar irradiation for 30 min.

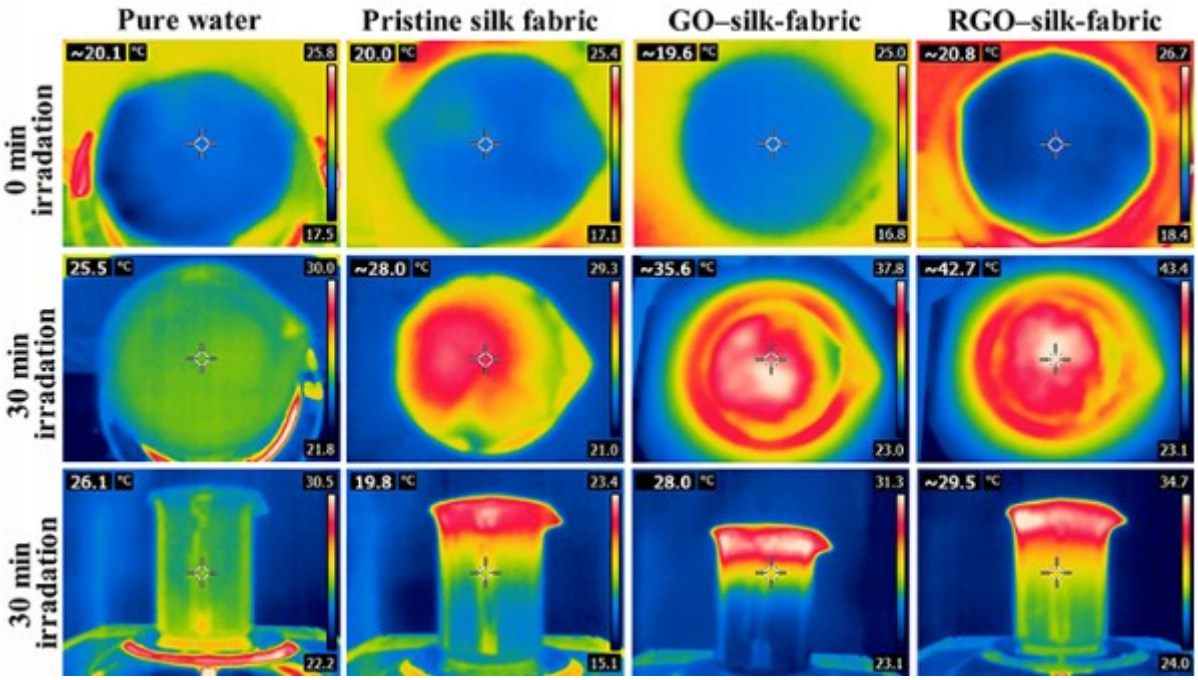

Fig. S9. Surface temperatures of pure water, pristine silk fabric, GO–silk-fabric, and RGO–silk-fabric before and after solar irradiation. The entire water-temperature distribution after irradiation was monitored by an infrared camera.

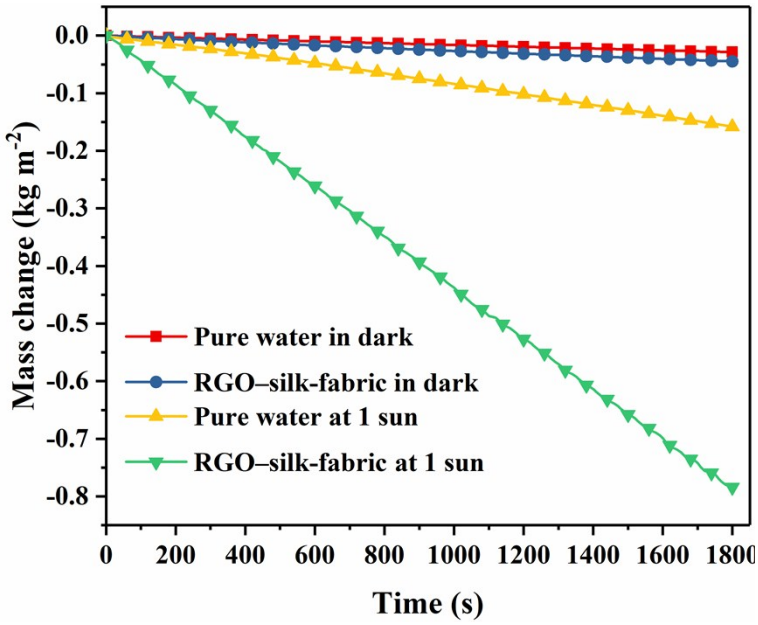

Fig. S10. Evaporation mass loss of water in dark and at 1 sun.

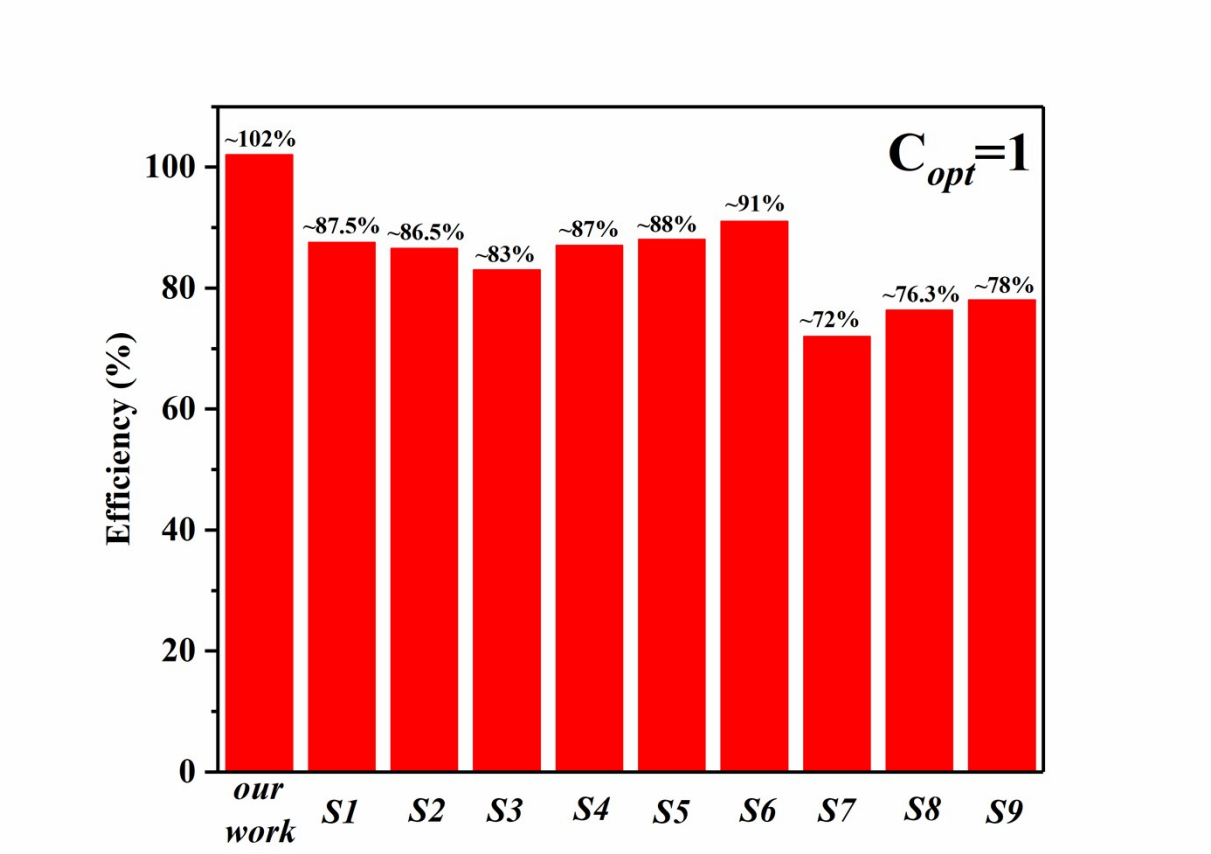

Fig. S11. Comparison of photothermal-conversion efficiencies of our samples and previously reported carbon materials under one sun irradiation.

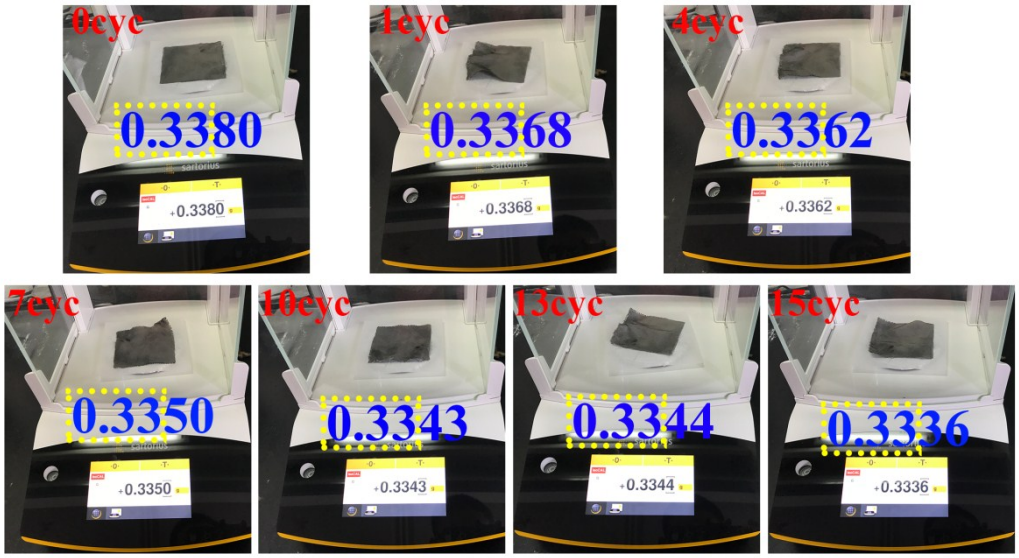

Fig. S12. The weight change of RGO-silk-fabric after cycles of use

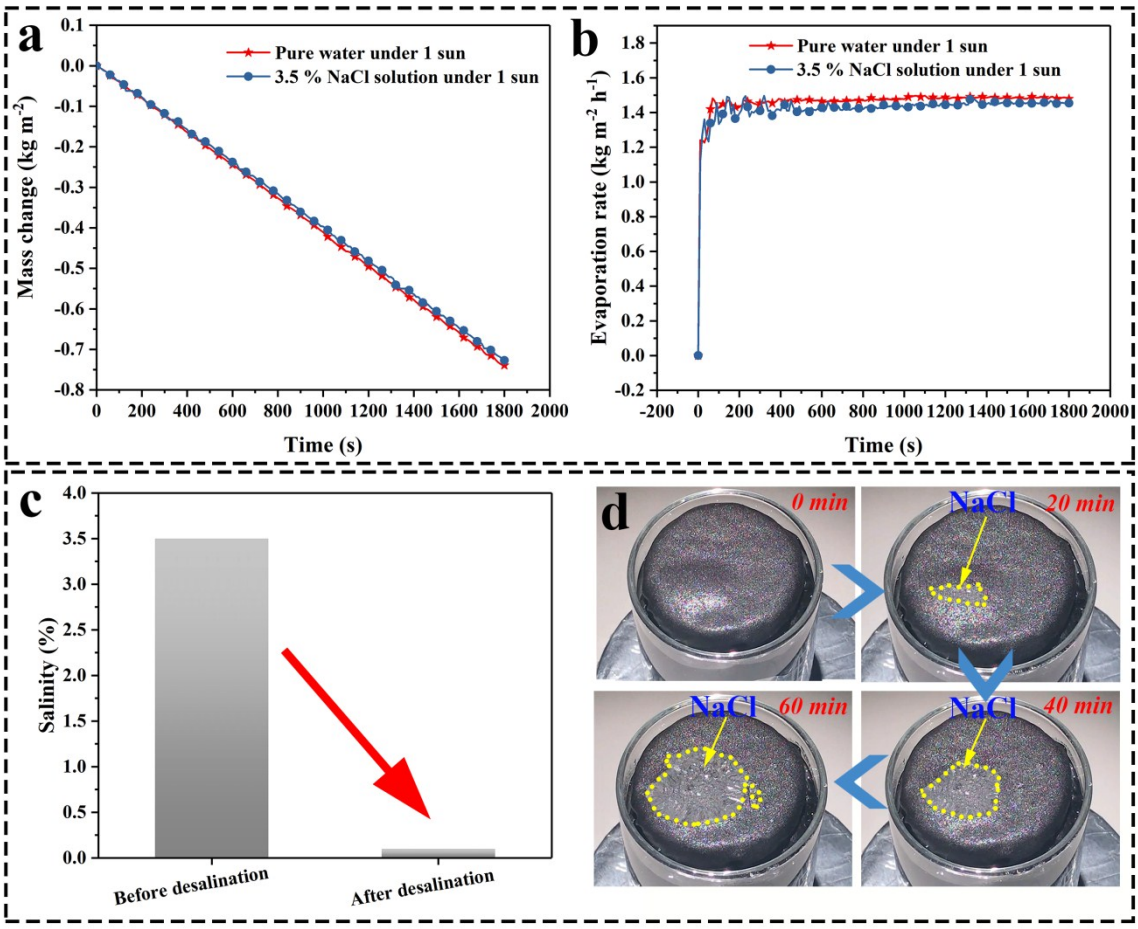

Fig. S13. (a) Evaporation mass loss of pure water and simulated seawater (3.5 wt% NaCl solution) with RGO-silk-fabric under one sun solar irradiation for 30 min; (b) the corresponding evaporation rate of pure water and simulated seawater (3.5 wt% NaCl solution); (c) the salt concentration comparison; (d) a progression of salt precipitation on the surface of RGO-silk-fabric under one sun solar.

Fig. S14. A refractometer used to test the concentration of the dissolved salt in water.

Table S1. Peak areas in C 1s spectra of GO–silk-fabric and RGO–silk-fabric.

Sample	Relative area corresponding to different chemical bonds (%)		
	C-C	C-O	C=O
GO–silk-fabric	60.25	28.30	11.45
RGO–silk-fabric	86.79	10.67	2.54

Table S2. Mechanical properties of pristine silk fabric and RGO–silk-fabric.

Sample	Strain at break (%)	Breaking strength (MPa)	Elastic modulus (MPa)
Pristine silk fabric	19.55±0.91	80.25±0.92	748.88±21.83
RGO–silk-fabric	16.67±1.53	72.22±5.55	774.96±15.48

The enhancement of the light absorption is attributed to the rough surface of materials, which can repeat light reflection or scattering and absorption inside materials' unique microstructures with unique structure.[S10-S12]

Supplementary References

1. Y. Li, T. Gao, Z. Yang, C. Chen, Y. Kuang, J. Song, C. Jia, E. M. Hitz, B. Yang and L. Hu, *Nano Energy*, 2017, **41**, 201-209.
2. P. Zhang, L. Jing, L. Lv, Z. Yang and L. Qu, *ACS Nano*, 2017, **11**, 5087–5093.
3. X. Hu, W. Xu, L. Zhou, Y. Tan, Y. Wang, S. Zhu and J. Zhu, *Adv. Mater.*, 2017, **29**, 1604031.
4. Y. Yang, R. Zhao, T. Zhang, K. Zhao, P. Xiao, Y. Ma, P. M. Ajayan, G. Shi and Y. Chen, *ACS Nano*, 2018, **12**, 829–835.
5. Z. Liu, H. Song, D. Ji, C. Li, Alec Cheney, Y. Liu, N. Zhang, X. Zeng, B. Chen, J. Gao, Y. Li, X. Liu, Diana Aga, S. Jiang, Z. Yu and Q. Gan, *Global Challenges*, 2017, **1**, 1600003.
6. X. Gao, H. Ren, J. Zhou, R. Du, C. Yin, R. Liu, H. Peng, L. Tong, Z. Liu and J. Zhang, *Chem. Mater.*, 2017, **29**, 5777–5781.
7. W. Xu, X. Hu, S. Zhuang, Y. Wang, X. Li, L. Zhou, S. Zhu and J. Zhu, *Adv. Energy Mater.*, 2018, 1702884.
8. F. Jiang, H. Liu, Y. Li, Y. Kuang, X. Xu, C. Chen, H. Huang, C. Jia, X. Zhao, Emily Hitz, Y. Zhou, R. Yang, L. Cui and L. Hu, *ACS Appl. Mater. Interfaces*, 2017, **10**, 1104–1112.
9. N. Xu, X. Hu, W. Xu, X. Li, L. Zhou, S. Zhu and J. Zhu, *Adv. Mater.*, 2017, **29**, 1606762.
10. J. D. Yao and G. W. Yang, *J. Mater. Chem. A,* 2018, **6**, 3869-3875.
11. J. D. Yao, Z. Q. Zheng and G. W.Yang, *Nanoscale,* 2018, **10**, 2876-2886.
12. J. D. Yao, Z. Q. Zheng and G. W. Yang, *Nanoscale,* 2017, **9**, 16396-16403.